Identification of the $1s2s2p\ ^4P_{5/2}\rightarrow 1s^22s\ ^2S_{1/2}$ magnetic quadrupole inner-shell satellite line in the Ar^{16+} *K*-shell x-ray spectrum

P. Beiersdorfer,[1] M. Bitter,[2] D. Hey,[1] and K. J. Reed[1]
[1]*Department of Physics and Advanced Technology, Lawrence Livermore National Laboratory, Livermore, California 94551*
[2]*Princeton Plasma Physics Laboratory, Princeton, New Jersey 08543*
(Received 19 December 2001; published 25 September 2002)

We have identified the dipole-forbidden $1s2s2p\ ^4P_{5/2}\rightarrow 1s^22s\ ^2S_{1/2}$ transition in lithiumlike Ar^{15+} in high-resolution *K*-shell x-ray emission spectra recorded at the Livermore EBIT-II electron-beam ion trap and the Princeton National Spherical Tokamak Experiment. Unlike other Ar^{15+} satellite lines, which can be excited by dielectronic recombination, the line is exclusively excited by electron-impact excitation. Its predicted radiative rate is comparable to that of the well-known $1s2p\ ^3P_1\rightarrow 1s^2\ ^1S_0$ magnetic quadrupole transition in heliumlike Ar^{16+}. As a result, it can also only be observed in low-density plasma. We present calculations of the electron-impact excitation cross sections of the innershell excited Ar^{15+} satellite lines, including the magnetic sublevels needed for calculating the linear line polarization. We compare these calculations to the relative magnitudes of the observed $1s2s2p\rightarrow 1s^22s$ transitions and find good agreement, confirming the identification of the lithiumlike $1s2s2p\ ^4P_{5/2}\rightarrow 1s^22s\ ^2S_{1/2}$ magnetic quadrupole line.

DOI: 10.1103/PhysRevA.66.032504 PACS number(s): 32.30.Rj, 34.80.Kw, 32.70.Fw, 52.70.La

I. INTRODUCTION

The lithiumlike dielectronic and collisional innershell satellite lines of the heliumlike *K*-shell x-ray spectra have been studied extensively in laboratory and astrophysical spectra. They provide information on the ionization equilibrium as well as electron temperature and density of the ambient plasma. In the case of solar and astrophysical plasma the lines are often the only means for determining these plasma parameters.

The *K*-shell lithiumlike satellite lines have in common that they originate from levels with energy above the heliumlike continuum threshold and therefore form autoionizing levels. The consequence is that their upper levels can be populated by dielectronic capture, i.e., by the inverse process of autoionization. Numerous calculations of dielectronic recombination from the $1s^2$ heliumlike ground state to levels of the type $1s2\ell 2\ell'$ have been carried out that predict the strength of dielectronic recombination and thus the intensity of the lithiumlike satellite lines populated by this process [1–5].

There are 16 possible $1s2\ell 2\ell'$ levels. These levels can decay by a total of 23 *K*-shell x-ray transitions. All radiative decays but one proceed via an electric dipole-allowed ($E1$) transition. These 22 $E1$ *K*-shell x-ray transitions were labeled alphabetically *a* through *v* by Gabriel [6].

The remaining transition is from the $1s2s2p\ ^4P_{5/2}$ level [7]. This level can decay to the $1s2s^2\ ^2S_{1/2}$, or the $1s^22s\ ^2S_{1/2}$ level. In either case, radiative decay from this level must proceed via a magnetic quadrupole ($M2$) transition. Decay to the $1s2s2p\ ^4P_{3/2}$ or $1s2s2p\ ^4P_{1/2}$ levels is also energetically possible. In these cases the radiative decay must proceed via a magnetic dipole ($M1$) or electric quadrupole ($E2$) transition.

The rates of $M2$, $M1$, or $E2$ transitions are much smaller than those of $E1$ transitions. As a result, dielectronic recombination into the $1s2s2p\ ^4P_{5/2}$ level, which is proportional to the radiative decay rate, is negligibly small compared to other lithiumlike *K*-shell satellite lines. It is, therefore, no surprise that the *K*-shell x-ray satellite corresponding to the $1s2s2p\ ^4P_{5/2}\rightarrow 1s2s^2\ ^2S_{1/2}$ transition is typically absent in tables of dielectronic satellite lines. In fact, Gabriel [6] did not label this transition when he introduced the alphabetical notation of the lithiumlike satellite lines.

The $1s2s2p\ ^4P_{5/2}$ level can also be excited by direct electron-impact excitation from the $1s^22s\ ^2S_{1/2}$ lithiumlike ground state. Nondipole excitation can be strong. In fact, collisionally pumped x-ray laser schemes, for example in neonlike systems, rely on large monopole and quadrupole excitation rates, and several electric quadrupole transitions have by now been identified [8–10]. Moreover, the well-known heliumlike transition $1s2p\ ^3P_2\rightarrow 1s^2\ ^1S_0$, labeled *x* in the notation of Gabriel [6] is strongly excited by electron impact from the ground state. The line is clearly visible in the *K*-shell spectra of heliumlike ions and has been used for diagnostic purposes [11–16]. Recent systematic calculations of the electron-impact excitation cross sections of various lithiumlike ions have omitted excitation to the $1s2s2p\ ^4P_{5/2}$ level [17]. However, earlier predictions were made by Bely-Dubau *et al.* for lithiumlike Fe^{23+} that the electron-impact excitation cross section of the $1s2s2p\ ^4P_{5/2}$ level from the lithiumlike ground state equals or exceeds that of other quartet levels as well as some of the doublet levels, in particular, those levels resulting in lines *s*, *t*, *u*, and *v* [18]. In the following, we present calculations of electron-impact excitation cross sections of the lithiumlike $1s2s2p$ levels in Ar^{15+} that confirm the trend set by the calculations for lithiumlike Fe^{23+} by Bely-Dubau *et al.* Lines *s*, *t*, *u*, and *v* have been observed in various studies of lithiumlike ions excitated by electron-impact collisions [19]. An equal or larger electron-impact excitation cross section for the $1s2s2p\ ^4P_{5/2}$ level thus suggests that the $M2$ line may also be observable.

The question whether the $M2$ decay of the lithiumlike $1s2s2p\ ^4P_{5/2}$ level can be detected also depends on the

TABLE I. Comparison of measured and predicted wavelengths of the innershell-excited Ar^{15+} satellite lines (in Å). The numbers in parentheses give the uncertainty in the last digits of the measured values.

Label	Transition	Wavelength[a]	Wavelength[b]	Wavelength[c]	Wavelength[d]	Wavelength[e]	Wavelength[f]
s	$1s2s2p\ ^2P_{3/2}\rightarrow 1s^22s\ ^2S_{1/2}$		3.9669	3.96738	3.9638	3.9680	3.96918
t	$1s2s2p\ ^2P_{1/2}\rightarrow 1s^22s\ ^2S_{1/2}$		3.9677	3.96659	3.9650	3.9685	3.97000
q	$1s2s2p\ ^2P_{3/2}\rightarrow 1s^22s\ ^2S_{1/2}$	3.98141(11)	3.9806	3.98370	3.9784	3.9827	3.98351
r	$1s2s2p\ ^2P_{1/2}\rightarrow 1s^22s\ ^2S_{1/2}$	3.98353(11)	3.9827	3.98150	3.9806	3.9851	3.98568
$M2$	$1s2s2p\ ^4P_{5/2}\rightarrow 1s^22s\ ^2S_{1/2}$	4.01211(15)	4.0114	4.01333	4.0123		
u	$1s2s2p\ ^4P_{3/2}\rightarrow 1s^22s\ ^2S_{1/2}$	4.01484(13)	4.0141	4.01607	4.0123	4.0165	4.01790
v	$1s2s2p\ ^4P_{1/2}\rightarrow 1s^22s\ ^2S_{1/2}$	4.01593(14)	4.0152	4.01719	4.0139	4.0176	4.01902

[a]Present measurement using EBIT-II.
[b]Vainshtein and Safronova, Ref. [1].
[c]Chen, Craseman, and Mark, Ref. [2].
[d]Bhalla and Tunnel, Ref. [3].
[e]Chen, Ref. [4].
[f]Nilsen, Ref. [5].

competing rate for Auger emission. Auger decay is not a competing process to the magnetic quadrupole radiation in neonlike and heliumlike ions. Auger decay of the $1s2\ell 2\ell'$ levels is typically very fast ($\geqslant 10^{12}$ s^{-1} in Ar^{15+}). Auger decay of the $1s2s2p\ ^4P_{5/2}$ level is, however, just as forbidden as radiative decay. Several studies have reported rates for the radiative or Auger decay of the $1s2s2p\ ^4P_{5/2}$ level. Bhalla and Tunnel calculated 1.63×10^9 s^{-1} for its Auger decay rate in Ar^{15+}; they calculated 3.18×10^8 s^{-1} for its K-shell radiative decay rate in Ar^{15+} [3]. The $2p\rightarrow 2p$ and $2p\rightarrow 2s$ L-shell radiative rates are negligibly small because of the small energy differences of the levels involved. As a result, their branching ratio for x-ray decay is 16.7%. Chen, Craseman, and Mark calculated 1.37×10^9 s^{-1} for its Auger decay rate and 3.16×10^8 s^{-1} for its K-shell radiative decay rate Ar^{15+}. Their predicted x-ray branching ratio is thus 18.7% [2]. Cheng, Lin, and Johnson calculated 1.46×10^9 s^{-1} for its Auger decay rate and 3.14×10^8 s^{-1} for its K-shell radiative decay rate Ar^{15+}, resulting in an x-ray branching ratio of 17.7% [20].

Beam-foil measurements of the lifetime of the $^4P_{5/2}$ level have been carried out on heavy-ion accelerators [21,22]. These have detected both Auger and radiative decay, and the wavelength of the $1s2s2p\ ^4P_{5/2}\rightarrow 1s^22s\ ^2S_{1/2}$ line in Ar^{15+} was measured to be 4.0124 ± 0.0009 Å [23–25]. Despite the fact that the radiative branching ratio is a few times smaller than many of the other innershell excited lithiumlike satellite lines, the $M2$ x-ray line should also be observable in collisional plasmas given its large collisional excitation rate. In fact, it may even be stronger than other lithiumlike lines provided that innershell excitation is the dominant excitation process and that the electron density is sufficiently low. Nevertheless, the $M2$ line has not yet been identified in the K-shell spectra of heliumlike ions from collisional plasmas to the best of our knowledge, despite the intense and systematic experimental scrutiny that these spectra have received in laboratory and astrophysical plasmas.

In the following we present measurements of the K-shell x-ray spectrum of heliumlike and lithiumlike argon that were performed on the Livermore EBIT-II electron-beam ion trap and the Princeton National Spherical Tokamak Experiment (NSTX). The electron-beam ion trap was operated at an electron-beam energy where direct electron-impact excitation was the only line formation mechanism so that only innershell excited satellites could be observed. The NSTX spectrum was collected from rather cold tokamak plasmas, as a low-electron temperature favors the excitation of the lithiumlike $M2$ line. In both spectra we were able to identify the lithiumlike $M2$ line. The line is comparable in intensity to that of the neighboring quartet lines u and v. A comparison of the relative intensity of the $M2$ line with calculated electron-impact excitation cross sections shows good agreement, and firmly establishes the identity of the lithiumlike $1s2s2p\ ^4P_{5/2}\rightarrow 1s^22s\ ^2S_{1/2}$ line.

II. THEORY

Systematic calculations of the atomic parameters of doubly excited lithiumlike levels along the isoelectronic sequence have been presented by a multitude of authors. Predictions of the wavelength of the $1s2s2p\rightarrow 1s^22s$ innershell-excited collisional satellite lines from some of these calculations are given in Table I. The calculations differ in the predicted wavelengths of the lithiumlike collisional satellite lines within about 5 mÅ. This means that the identification of the $M2$ line by wavelength alone is, in principle, uncertain given that it is within 5 mÅ of neighboring lines u and v as well as the collisional satellite transition $1s2s^22p\ ^1P_1\rightarrow 1s^22s^2\ ^1S_0$ in berylliumlike Ar^{14+}, commonly labeled β. However, the calculations are consistent in predicting that the $M2$ line has a wavelength that is a few mÅ shorter than either line u or line v. Hence, the calculations help in the identification of the $M2$ transition provided lines u and v are identified.

To assess the relative intensities of the $1s2s2p\rightarrow 1s^22s$ collisional satellite lines, we performed distorted-wave cal-

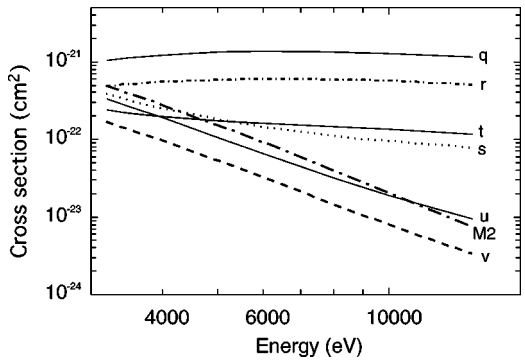

FIG. 1. Electron-impact excitation cross sections for populating the upper levels of the lithiumlike innershell satellite lines q, r, s, t, u, v, and the $M2$ line.

culations of the electron-impact excitation cross sections using the relativistic computer code developed by Zhang, Sampson, and Clark [26]. The results are shown in Fig. 1. The calculations show that the cross section for excitation of the $M2$ line ties with that of line r for second place at threshold. It reaches fully one third of the cross section for line q. Line q has been observed in all K-shell spectra with the proper ionization balance. Unlike the cross section for excitation of line q and that of the other lines emanating from doublet-P levels, the cross section of the $M2$ line falls rapidly with increasing electron energy because of the nondipole nature of the excitation. In doing so it follows the trend set by the excitation cross sections of the other two quartet lines u and v. From the energy dependence of its cross section it is clear that the intensity of the $M2$ line is strongest in colder plasmas where the line emission is dominated by the excitation cross section at and just above threshold.

A summary of the predicted radiative and autoionization decay rates of the $1s2s2p\ ^4P_{5/2} \rightarrow 1s^2 2s\ ^2S_{1/2}$ transition is given in Table II. The radiative rate is only two orders of magnitude larger than that associated with the well-known magnetic dipole line z in heliumlike Ar^{16+}. The heliumlike magnetic dipole rate has been calculated and measured to be about 5×10^6 s^{-1} [27,28]. By contrast, the magnetic quadrupole rate of line x has been calculated to be 3.16×10^8 s^{-1} [27], which is essentially identical to that of the radiative decay rate of the $1s2s2p\ ^4P_{5/2}$ level.

TABLE II. Calculated radiative decay rates A_r and Auger decay rates A_a of the $1s2s2p\ ^4P_{5/2} \rightarrow 1s^2 2s\ 2S_{1/2}$ transition.

A_r (s^{-1})	A_a (s^{-1})	References
3.16[8]	1.37[9]	[2]
3.18[8]	1.63[9]	[3]
3.14[8]	1.46[9]	[20]

A summary of the predicted radiative branching ratios (K-shell fluorescent yield), β_r, of the $1s2s2p\ ^4P_{5/2} \rightarrow 1s^2 2s\ ^2S_{1/2}$ transition is given in Table III. The average predicted radiative branching ratio is about 17%.

The predicted radiative branching ratios associated with the other innershell-excited lithiumlike satellite lines are also shown in Table III. The values exhibit a wide range. For example, for satellite s β_r ranges from 0.05 to 0.21; for r the range is 0.78–0.91, and for u it is 0.61–0.99.

The radiative branching ratios are needed in conjunction with the calculated electron-impact excitation rates for predicting the intensity of the various collisional satellite lines. The spread in β_r carries over to the intensity predictions and adds uncertainties to these predictions. In Fig. 2 we show the effective cross section for x-ray production, i.e., $\beta_r\sigma$, for the different lines. Here, σ is the cross section shown in Fig. 1. For β_r we used the average of the last four of the five calculations listed in Table III. We did not include the values calculated by Vainshtein and Safronova [1] in the average, because their values differed the most from the average.

The curves in Fig. 2 provide a direct measure of the intensity of each collisional satellite line. Because the radiative branching ratio of the $M2$ line is a few times less than that of most other collisional satellite lines, the lithiumlike $M2$ line is predicted to be only the fifth strongest line near threshold for electron-impact excitation, and it is predicted to be the smallest of the three quartet transitions.

TABLE III. Calculated radiative branching ratios of the innershell-excited $1s2s2p \rightarrow 1s^2 2s$ Ar^{15+} satellite lines.

Label	β_r [a]	β_r [b]	β_r [c]	β_r [d]	β_r [e]
s	0.206	0.052	0.050	0.067	0.048
t	0.369	0.174	0.175	0.195	0.180
q	0.950	0.973	0.975	0.942	0.963
r	0.798	0.841	0.864	0.784	0.901
$M2$		0.187	0.163		
u	0.614	0.974	0.843	0.988	0.871
v	0.711	0.944	0.853	0.911	0.992

[a]Vainshtein and Safronova, Ref. [1].
[b]Chen, Craseman, and Mark, Ref. [2].
[c]Bhalla and Tunnel, Ref. [3].
[d]Chen, Ref. [4].
[e]Nilsen, Ref. [5].

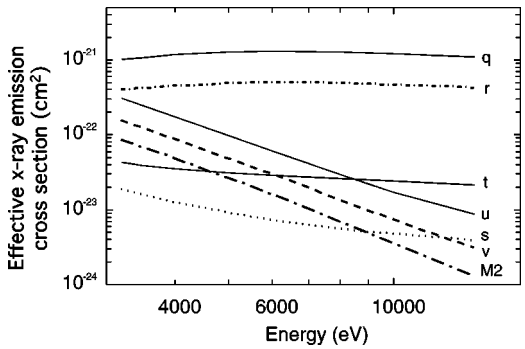

FIG. 2. Effective electron-impact excitation cross sections for producing x-ray emission from the lithiumlike innershell satellite lines q, r, s, t, u, v, and the $M2$ line. The calculations utilize the cross sections from Fig. 1 and the average branching ratio of the last four entries in Table III, as described in the text.

Lines excited in an electron-beam ion trap are generally linearly polarized because of the directionality introduced in the excitation process by the electron beam [29]. The amount of polarization can be calculated from the values of the magnetic sublevel cross sections [30]. These cross sections are provided by our distorted-wave calculation using the computer code by Zhang, Sampson, and Clark [26]. The resulting values of linear polarization of each of the seven collisional satellite lines are shown as a function of electron collision energy in Fig. 3. The calculations show that lines q and s are strongly positively polarized near threshold, while line u and the $M2$ line are strongly negatively polarized. The remaining lines are unpolarized. The reason for the strictly vanishing polarization is that they emanate from upper levels with total angular momentum $J=1/2$ and therefore cannot be linearly polarized.

III. MEASUREMENTS

The measurements were carried out both on the EBIT-II electron-beam ion trap and the NSTX tokamak. EBIT-II is the second electron-beam ion trap constructed. It was put into operation at the Lawrence Livermore national laboratory in 1990. NSTX at the Princeton Plasma Physics Laboratory represents a novel design for testing plasma operation in a low-aspect ratio machine. Both devices operate at low electron density, $\leqslant 3\times10^{13}$ cm^{-3} in NSTX and $\leqslant 5\times10^{12}$ cm^{-3} in EBIT-II.

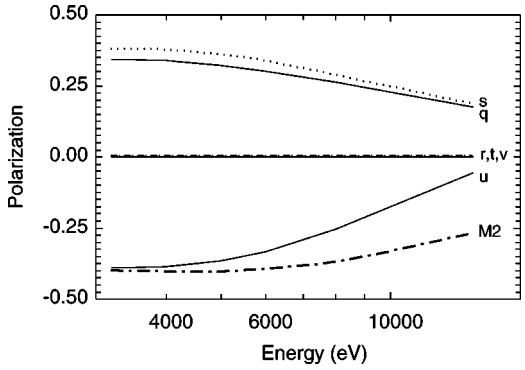

FIG. 3. Calculated values of the linear polarization of the lithiumlike innershell satellite lines q, r, s, t, u, v, and the $M2$ line.

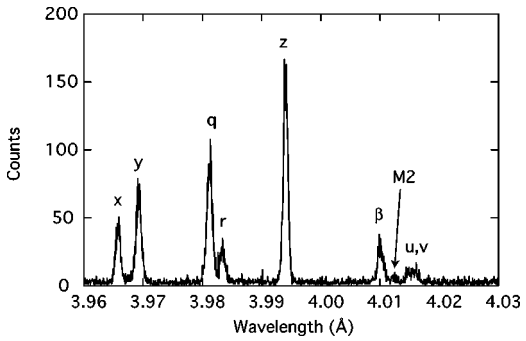

FIG. 4. K-shell emission spectrum of argon obtained with the high-resolution von Hámos crystal spectrometer on EBIT-II showing the Ar^{16+} lines x, y, and z, the Ar^{15+} lines q, r, u, v, and the $M2$ line, and the Ar^{14+} line β. The spectrum was obtained at a constant electron-beam energy 200 eV above threshold for electron-impact excitation.

A. Electron-beam ion trap measurements

The EBIT-II measurements utilized a high-resolution crystal spectromer in the von Hámos geometry [31,32]. The spectrometer employed a quartz $(11\bar{2}0)$ crystal bent to a radius of curvature of 75 cm and a multiwire proportional counter. The lattice spacing of the crystal was $2d=4.912$ Å. The Bragg angle was 54°. The quartz crystal provided high-intrinsic resolution not afforded by other crystals such as LiF. Moreover, its crystalline structure is close to that of a perfect crystal so that corrections for polarization-dependent reflectivities are readily made.

Spectra recorded on EBIT-II are shown in Figs. 4 and 5. The measurement in Fig. 4 was made by setting the energy of the electron beam to a value about 200 eV above threshold for electron-impact excitation. At this energy electron-impact excitation is the dominant excitation process of the lines. The spectrum shows the heliumlike lines x and z as well as the

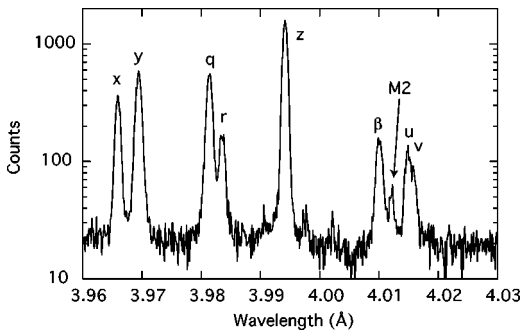

FIG. 5. K-shell emission spectrum of argon obtained with the high-resolution von Hámos crystal spectrometer on EBIT-II showing the Ar^{16+} lines x, y, and z, the Ar^{15+} lines q, r, u, v, and the $M2$ line, and the Ar^{14+} line β. The spectrum was obtained by sweeping the electron-beam energy from threshold to 300 eV above threshold for electron-imapct excitation. The spectrum is displayed on a logarithmic scale to enhance the weaker lines.

intercombination line *y* corresponding to the transition $1s2p\ ^1P_1 \rightarrow 1s^2\ ^1S_0$. It also shows the berylliumlike line β and the lithiumlike innershell lines *q*, *r*, *u*, and *v* as well as the $M2$ line. The latter is the smallest feature in the spectrum. By contrast, lines *s* and *t* cannot be discerned. These lines are located close to line *y* and are predicted to be even weaker than the $M2$ line (cf. Fig. 2).

The same set of lines can be seen in the spectrum in Fig. 5, which was recorded by sweeping the electron-beam energy from threshold to 300 eV above threshold. The $M2$ line is again the weakest line in the spectrum, although it is clearly visible and fully resolved.

We used the two data sets to determine the wavelength of the lithiumlike innershell satellite lines. The results are shown in Table I. The wavelength scale of the EBIT-II measurements was established by setting the wavelengths of lines *x* and *z* to those calculated by Drake [33], which have been shown to be accurate [34]. This procedure combined with nonlinearities in the position-sensitive proportional counter introduces a systematic uncertainty of 0.1 mÅ in our wavelength measurements. This error combines with the statistical errors in our line fitting procedures to produce the uncertainties listed in Table I.

Our measured wavelength of the $1s2s2p\ ^4P_{5/2} \rightarrow 1s^2 2s\ ^2S_{1/2}$ line of $4.012\,11 \pm 0.000\,15$ Å agrees within uncertainty limits with the value of 4.0124 ± 0.0009 Å measured in beam-foil experiments [24]. Our result is, however, much more accurate.

Comparing our measured wavelengths to those listed in Table I we find that the wavelengths calculated by Vainshtein and Safronova [1] best reproduce the measured values. Those by Nilsen [5] differ the most from the measured values.

The intensity of the $M2$ line in the EBIT-II measurements was suppressed by the fact that the line is negatively polarized. The spectrometer recorded the x-ray emission in the plane perpendicular to the electron beam. In this arrangement, the intensity of negatively polarized lines is suppressed by a factor of $3/(3-P)$, where P is the line's polarization. Moreover, the crystal reflects negatively polarized radiation with less efficiency than positively polarized radiation, as described in [29,30]. On the other hand, line *q*, which is positively polarized, is enhanced. The polarization effects combine to suppress the ratio of the $M2$ intensity to that of *q* by a factor of 1.97.

In Fig. 6 we show the predicted relative intensities of the lithiumlike collisional satellite lines relative to that of line *q* as a function of the electron-impact excitation energy. These calculations are based on the data presented in Fig. 2. For comparison we also show the ratios measured on EBIT-II. These values are weighted averages of the two measurements shown in Figs. 4 and 5 and are adjusted for polarization effects.

The comparison between the measured intensities using EBIT-II and the predictions is good. The small differences are well within the uncertainties of the theoretical data. Together with the match in the experimental and theoretical wavelengths, the good agreement in the relative intensities of the $M2$ line provides positive identification of the $M2$ line.

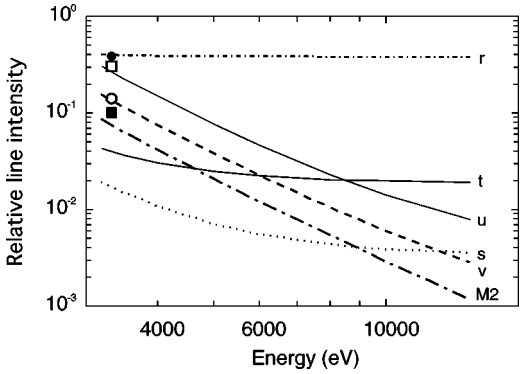

FIG. 6. Comparison of the predicted and measured relative intensities of the lithiumlike collisional satellite lines. The intensities are normalized to that of line *q*. The solid circle denotes the measured value for line *r*, the open square line *u*, the open circle line *v*, and the solid square the $M2$ line.

B. Tokamak measurements

Like the EBIT-II measurements, the NSTX measurements utilized a quartz $(11\bar{2}0)$ crystal. The crystal was spherically bent to a radius of 3.75 m and employed in a Johann-type geometry [35]. A multiwire position-sensitive proportional counter was used to detect the reflected x rays.

The measurements were carried out during the ohmic heating phase. The central NSTX electron density was about 3×10^{13} cm^{-3}; the central electron temperature reached about 0.7 keV. This temperature was sufficiently low so that a large fraction of the argon was in the lithiumlike charge state. Moreover, the temperature is sufficiently low so that collisional excitation is dominated by electrons with energy near the excitation threshold.

A spectrum from NSTX showing the Ar^{15+} lines is shown in Fig. 7. The spectrum shows the same lines as the EBIT-II spectra in Figs. 4 and 5 as well as three additional lines. The additional lines are the Ar^{15+} satellite lines *a*, *j*, and *k*, whereby line *j* blends with line *z* and greatly enhances its intensity. These lines are excited only by dielectronic recombination at a distinct resonance energy several hundred eV

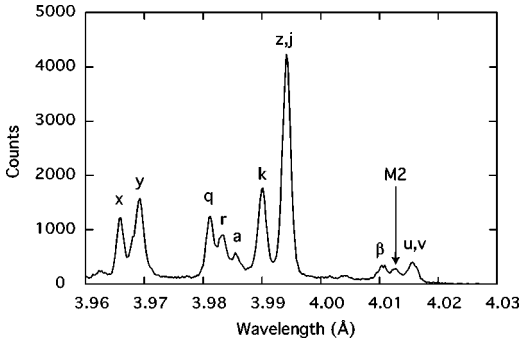

FIG. 7. *K*-shell emission spectrum of argon obtained with the high-resolution von Johann crystal spectrometer on NSTX showing the Ar^{16+} lines *x*, *y*, and *z*, the Ar^{15+} lines *q*, *r*, *u*, *v*, and the $M2$ line, as well as the pure dielectronic satellite lines *a*, *j*, and *k*, and the Ar^{14+} line β. The spectrum was obtained at a plasma temperature of about 700 eV.

below threshold for direct electron-impact excitation of the collisional satellite lines. The lines were absent in the EBIT-II spectra where the electron-beam energy was far away from the relevant dielectronic resonance energies.

The dielectronic satellite lines *a*, *j*, and *k* have been seen in a variety of tokamak measurements [16,36,37], as dielectronic recombination is one of the dominant line excitation mechanisms in tokamak plasmas. Dielectronic recombination also plays a role in exciting some of the other Ar^{15+} satellite lines, especially line *r*. In addition, the spectrum contains weak, unresolved dielectronic satellite lines that blend with the various features, including *q* and *y*.

Unlike the EBIT-II spectra, the NSTX line intensities are unaffected by polarization effects because electron collisions are isotropic in an ohmically heated tokamak. As a result, the intensity of the $M2$ line does not suffer the decrease it experienced in the EBIT-II measurements. It is clearly seen between the berylliumlike resonance line β and the blend of satellites *u* and *v*. The latter were situated near the edge of the wavelength range spanned by the spectrometer. No further x-ray flux is, therefore, observed on the long-wavelength side of those two quartet lines.

IV. CONCLUSIONS

Using high-resolution spectroscopy of low-temperature tokamak plasmas and the capabilities to select excitation processes with the electron-beam ion trap device we have identified the $1s2s2p\ ^4P_{5/2}\rightarrow 1s^2 2s\ ^2S_{1/2}$ dipole-forbidden collisional satellite line. All other $1s2s2p\rightarrow 1s^2 2s$ collisional satellite lines had been earlier identified in the *K*-shell spectra of highly charge heliumlike ions. The newly identified magnetic quadrupole line joins only two other dipole-forbidden lines that are known to exist in the *K*-shell spectra of heliumlike ions, i.e., lines *x* and *z*.

Detailed calculations were presented that supported the identification of the line. Collisional excitation is the only formation process of this line. Its electron-impact excitation cross section drops off rapidly as a function of electron energy, while that of the lithiumlike resonance line *q* increases. This suggests using the ratio of the intensity of the $M2$ line (and that of *u* and *v*) to that of line *q* as an electron temperature diagnostic.

The line was also shown to be strongly negatively polarized when excited by an electron beam. This suggests that it will be easier to detect this line using an electron-beam ion trap if the plane of dispersion were rotated by 90° from the plane used in our measurements.

We measured its wavelength and noted that its intensity is comparable to that of the other quartet lines *u* and *v*. The plasma observations show that the line is readily observed under conditions where sufficient amounts of lithiumlike ions are produced. In fact, the lithiumlike $M2$ line was observed on the NSTX tokamak to have the same intensity as the neighboring berylliumlike resonance line β.

In many astrophysical and laboratory measurements the ratios of the heliumlike, lithiumlike, and berylliumlike resonance lines *w*, *q*, and β are used to determine the ionization balance and thus to infer the plasma electron temperature or transport parameters. We predict that the $M2$ satellite line blends with line β in the *K*-shell spectrum of Fe^{24+}. Given that the $M2$ line can assume an intensity comparable to that of β, such a blending would lead to the wrong inferred ionization balance, and in turn a wrong inferred electron temperature. This is a special concern in the study of astrophysical plasmas where no independent, nonspectroscopic electron temperature diagnostic is available. Identification of this line and a detailed study of its effects in astrophysically relevant *K*-shell spectra will be necessary.

ACKNOWLEDGMENTS

We thank Dr. M. H. Chen for valuable discussions. This work was supported in part by the Office of Fusion Energy Sciences as part of the Basic and Applied Plasma Science initiative. Work by the University of California Lawrence Livermore National Laboratory was performed under the auspices of the Department of Energy under Contract No. W-7405-Eng-48; work by the Princeton University Plasma Physics Laboratory was performed under the auspices of the Department of Energy under Contract No. DE-AC02-76CHO3073.

[1] L.A. Vainshtein and U.I. Safronova, At. Data Nucl. Data Tables **25**, 49 (1978).
[2] M.H. Chen, B. Crasemann, and H. Mark, Phys. Rev. A **24**, 1852 (1981).
[3] C.P. Bhalla and T.W. Tunnell, J. Quant. Spectrosc. Radiat. Transf. **32**, 141 (1984).
[4] M.H. Chen, At. Data Nucl. Data Tables **34**, 301 (1986).
[5] J. Nilsen, At. Data Nucl. Data Tables **38**, 339 (1988).
[6] A.H. Gabriel, Mon. Not. R. Astron. Soc. **160**, 99 (1972).
[7] J.L. Pietenpol, Phys. Rev. Lett. **7**, 64 (1961).
[8] D.D. Dietrich, G.A. Chandler, R.J. Fortner, C.J. Hailey, and R.E. Stewart, Phys. Rev. Lett. **54**, 1008 (1985).
[9] P. Beiersdorfer, M. Bitter, S. von Goeler, S. Cohen, K.W. Hill, J. Timberlake, R.S. Walling, M.H. Chen, P.L. Hagelstein, and J.H. Scofield, Phys. Rev. A **34**, 1297 (1986).
[10] P. Beiersdorfer, S. von Goeler, M. Bitter, E. Hinnov, R. Bell, S. Bernabei, J. Felt, K.W. Hill, R. Hulse, J. Stevens, S. Suckewer, J. Timberlake, A. Wouters, M.H. Chen, J.H. Scofield, D.D. Dietrich, M. Gerassimenko, E. Silver, R.S. Walling, and P.L. Hagelstein, Phys. Rev. A **37**, 4153 (1988).
[11] J.E. Rice, E.S. Marmar, E. Källne, and J. Källne, Phys. Rev. A **35**, 3033 (1987).
[12] F.P. Keenan and S.M. McCann, J. Phys. B **23**, L423 (1990).
[13] K.-D. Zastrow, E. Källne, and H.P. Summers, Phys. Rev. A **41**, 1427 (1990).
[14] J.E. Rice, M.A. Graf, J.L. Terry, E.S. Marmar, K. Giesing, and F. Bombarda, J. Phys. B **28**, 893 (1995).
[15] L.K. Harra-Murnion, K.J.H. Phillips, J.R. Lemen, D.M. Zarro, C.J. Greer, V.J. Foster, R. Barnsley, I.H. Coffey, J. Dubau, F.P. Keenan, E. Rachlew-Källne, T. Watanabe, and M. Wilson, As-

tron. Astrophys. **306**, 670 (1996).
[16] G. Bertschinger, W. Biel, TEXTOR-94 Team, O. Herzog, J. Weinheimer, H.-J. Kunze, and M. Bitter, Phys. Scr., T **T83**, 132 (1999).
[17] U.I. Safronova, M.S. Safronova, and T. Kato, Phys. Scr. **54**, 68 (1996).
[18] F. Bely-Dubau, J. Dubau, P. Faucher, and A.H. Gabriel, Mon. Not. R. Astron. Soc. **198**, 239 (1982).
[19] K.L. Wong, P. Beiersdorfer, K.J. Reed, and D.A. Vogel, Phys. Rev. A **51**, 1214 (1995).
[20] K.-T. Cheng, C.-P. Lin, and W.R. Johnson, Phys. Lett. A **48**, 437 (1974).
[21] I.A. Sellin, Adv. At. Mol. Phys. **12**, 215 (1976).
[22] H.G. Berry, Rep. Prog. Phys. **40**, 155 (1977).
[23] H.D. Dohmann, D. Liesen, and H. Pfeng, Z. Phys. A **285**, 171 (1978).
[24] H.D. Dohmann and H. Pfeng, Z. Phys. A **288**, 29 (1978).
[25] H.D. Dohmann and R. Mann, Z. Phys. A **291**, 15 (1979).
[26] H.L. Zhang, D.H. Sampson, and R.E.H. Clark, Phys. Rev. A **41**, 198 (1990).
[27] C.D. Lin, W.R. Johnson, and A. Dalgarno, Phys. Rev. A **15**, 154 (1977).
[28] S. Cheng, R.W. Dunford, C.J. Lui, B.J. Zabransky, A.E. Livingston, and L.J. Curtis, Phys. Rev. A **49**, 2347 (1994).
[29] P. Beiersdorfer, in *Proceedings of the US-Japan Workshop and International Seminar on Plasma Polarization Spectroscopy, Kyoto, Japan, 1998*, NIFS-PROC-37, edited by T. Fujimoto and P. Beiersdorfer (National Institute for Fusion Science, Toki, 1998), pp. 67–89.
[30] P. Beiersdorfer, D.A. Vogel, K.J. Reed, V. Decaux, J.H. Scofield, K. Widmann, G. Hölzer, E. Förster, O. Wehrhan, D.W. Savin, and L. Schweikhard, Phys. Rev. A **53**, 3974 (1996).
[31] P. Beiersdorfer, R.E. Marrs, J.R. Henderson, D.A. Knapp, M.A. Levine, D.B. Platt, M.B. Schneider, D.A. Vogel, and K.L. Wong, Rev. Sci. Instrum. **61**, 2338 (1990).
[32] P. Beiersdorfer, in *X-Ray and Innershell Processes*, edited by R.L. Johnson, H. Schmidt-Böcking, and B.F. Sonntag, AIP Conf. Proc. No. 389 (AIP, Woodbury, NY, 1997), p. 121.
[33] G.W.F. Drake, Can. J. Phys. **66**, 586 (1988).
[34] P. Beiersdorfer, M. Bitter, S. von Goeler, and K.W. Hill, Phys. Rev. A **40**, 150 (1989).
[35] M. Bitter, K.W. Hill, A.L. Roquemore, P. Beiersdorfer, S.M. Kahn, S.R. Elliott, and B. Fraenkel, Rev. Sci. Instrum. **70**, 292 (1999).
[36] TFR Group, M. Cornille, J. Dubau, and M. Loulergue, Phys. Rev. A **32**, 3000 (1985).
[37] TFR Group, F. Bombarda, F. Bely-Dubau, P. Faucher, M. Cornille, J. Dubau, and M. Loulergue, Phys. Rev. A **32**, 2374 (1985).